

MIT Open Access Articles

*Efficient terahertz generation in highly
nonlinear organic crystal HMB-TMS*

The MIT Faculty has made this article openly available. **Please share**
how this access benefits you. Your story matters.

Citation: Lu, Jian, Seung-Heon Lee, Xian Li, Seung-Chul Lee, Jae-Hyun Han, O-Pil Kwon, and Keith A. Nelson. "Efficient Terahertz Generation in Highly Nonlinear Organic Crystal HMB-TMS." Optics Express 26, no. 23 (November 8, 2018): 30786.

As Published: <http://dx.doi.org/10.1364/OE.26.030786>

Publisher: Optical Society of America

Persistent URL: <http://hdl.handle.net/1721.1/121073>

Version: Final published version: final published article, as it appeared in a journal, conference proceedings, or other formally published context

Terms of Use: Article is made available in accordance with the publisher's policy and may be subject to US copyright law. Please refer to the publisher's site for terms of use.





Efficient terahertz generation in highly nonlinear organic crystal HMB-TMS

JIAN LU,^{1,3} SEUNG-HEON LEE,^{2,3} XIAN LI,¹ SEUNG-CHUL LEE,²
JAE-HYUN HAN,² O-PIL KOWN^{2,4} AND KEITH A. NELSON^{1,*}

¹Department of Chemistry, Massachusetts Institute of Technology, Cambridge, Massachusetts 02139, USA

²Department of Molecular Science and Technology, Ajou University, Suwon 443-749, South Korea

³These authors contributed equally to the paper.

⁴opilkwon@ajou.ac.kr

*kanelson@mit.edu

Abstract: We report on generation of strong and broadband terahertz (THz) pulses via collinearly phase-matched optical rectification of near-infrared femtosecond pulses in the organic nonlinear optical HMB-TMS (2-(4-hydroxy-3-methoxystyryl)-3-methylbenzo[d]thiazol-3-ium 2,4,6-trimethylbenzenesulfonate) single crystals which exhibit optimal molecular orientation and large macroscopic optical nonlinearity for efficient THz wave generation. Single-cycle THz pulses with a peak electric field strength of 0.66 MV/cm and a bandwidth from 0.1 to 5.4 THz are achieved from an HMB-TMS crystal with only a 2-mm clear aperture pumped by 1350 nm pulses at moderate fluences. The generated THz energy is about 1 μ J and the corresponding pump-to-THz energy conversion efficiency reaches 0.23%.

© 2018 Optical Society of America under the terms of the [OSA Open Access Publishing Agreement](#)

1. Introduction

The rapid progress of strong terahertz (THz) pulse generation techniques has enabled THz nonlinear spectroscopy and control of various material degrees of freedom in a plethora of systems which are relevant for condensed-matter physics, chemistry and biology [1, 2]. The study of linear and nonlinear THz light-matter interactions has enabled the observation of intriguing physics such as insulator-to-metal phase transitions in correlated electron materials [3], spectroscopic studies of nonlinear rotational dynamics of gas-phase molecules [4, 5], vibrational dynamics in solids and liquids [6, 7], spin dynamics in magnetic materials [8–10], and very recently, multidimensional THz spectroscopy of these rotational, vibrational and spin degrees of freedom [11–13]. In these examples, the THz sources are often based on optical rectification (OR) of femtosecond (fs) laser pulses in LiNbO₃ crystals which is capable of generating strong THz pulses with energy approaching mJ [14–17]. However, certain drawbacks exist in LiNbO₃-based THz sources. Firstly, experimental complication arises, as a noncollinear phase matching method is required to compensate the huge index mismatch between the optical and THz pulses [18]. Secondly, with the noncollinear phase matching method, LiNbO₃-based THz sources only cover the frequency region between 0.1 and 3 THz, beyond which a strong high-lying phonon deteriorates the generation efficiency. Thirdly, optimized pump pulse duration and wavelength, and cryogenic cooling are required to further increase the THz generation efficiency at the cost of reduced bandwidth [19, 20]. Methods based on nonlinear frequency mixing of fs laser pulses in gases can provide intense THz pulses with broad bandwidth covering the entire far-infrared regime [21], but the relatively weak spectral brightness limits their applications in nonlinear THz spectroscopy. THz pulses that can provide broad bandwidth and strong spectral brightness are highly desired for applications in linear and nonlinear THz spectroscopy and THz optics.

Recently, alternative approaches for strong and broadband THz generation based on OR in organic nonlinear optical crystals have proven very promising [22]. Such organic single crystals typically exhibit higher second-order optical nonlinearity compared to benchmark inorganic

crystals and usually show high optical quality and good crystal characteristics for THz wave generation [23]. Owing to the good THz and near-infrared (NIR) optical transparency and excellent index matching between NIR and THz fields, benchmark organic crystals including DAST (4-(4-(N,N-dimethylamino)styryl)-1-methylpyridinium 4-methylbenzenesulfonate), DSTMS (4-(4-(N,N-dimethylamino)styryl)-1-methylpyridinium 2,4,6-trimethylbenzenesulfonate), HMQ-TMS (2-(4-hydroxy-3-methoxystyryl)-1-methylquinolinium 2,4,6-trimethylbenzenesulfonate) and OH1 (2-(3-(4-hydroxystyryl)-5,5-dimethylcyclohex-2-enylidene)malononitrile) have been demonstrated to generate strong THz pulses with up to GV/m level electric field strength and broad bandwidth [22, 24–26]. These achievements have stimulated considerable efforts in the development of new organic crystals by chemical modifications for intense THz generation [27]. Recently, we have reported a new class of organic crystals based on a benzothiazolium electron-acceptor which proves stronger nonlinearity than the two classes of benchmark organic crystals based on either pyridinium (e.g., DAST and DSTMS) or quinolinium (e.g., HMQ-TMS) [28]. When pumped by laser pulses at 800 nm, the newly developed HMB-TMS (2-(4-hydroxy-3-methoxystyryl)-3-methylbenzo[d]thiazol-3-ium 2,4,6-trimethylbenzenesulfonate) crystals with a small clear aperture (2 mm) are capable of generating THz pulses that have an order of magnitude higher field strength (up to 100 kV/cm) and broader bandwidth (up to 5.3 THz) than the inorganic ZnTe crystals under the same condition [28]. The THz generation efficiency of HMB-TMS crystals might be improved with better phase matching condition between optical and THz frequencies by controlling the pump frequencies and crystal thicknesses. The promising potential of efficient THz generation in HMB-TMS crystals warrants further investigation.

In this report, we present a systematic study of the THz generation characteristics in HMB-TMS crystals with various crystal thicknesses at pump wavelength from 1200 nm to 1450 nm. We characterized the optical group indices at selected wavelengths in the NIR regime and the THz absorption coefficients and refractive indices of the HMB-TMS crystals, which allowed us to estimate the optimum crystal lengths for THz generation pumped by NIR fs pulses. The calculated long optimum crystal lengths permitted OR with good phase matching in a straightforward collinear geometry. Measurements of the generated THz fields from HMB-TMS crystals with different thicknesses pumped by NIR fs pulses at selected wavelengths allowed the determination of the optimal pump wavelength and crystal thickness. Particularly, a small size (2-mm diameter) 0.4-mm thick HMB-TMS crystal pumped by NIR fs pulses at 1350 nm produced single-cycle THz pulses with a peak electric field strength of 0.64 MV/cm and a broad bandwidth up to 5.4 THz. The generated THz energy was about 1 μ J and the corresponding optical pump-to-THz energy conversion efficiency was about 0.23%.

2. Phase matching condition for THz generation

For efficient THz wave generation by OR, the generation nonlinear crystals require various linear and nonlinear optical properties; e.g., large second-order nonlinearity, small absorption at the optical pump and THz frequencies, and good phase matching between the pump and THz fields (i.e., index matching). We firstly consider linear and nonlinear optical properties of HMB-TMS crystals in optical and THz frequency regions.

The chemical structure of HMB-TMS is shown in Fig. 1(a). HMB-TMS crystals with large sizes that is essential for intense THz generation can be routinely grown by solution growth methods [28]. A photograph of a cleaved HMB-TMS crystal is shown in Fig. 1(b), which exhibits parallel crystal surfaces and good optical quality. In general, the polar axis of nonlinear optical crystals is defined as the average direction of the maximal first-order hyperpolarizability β_{\max} of the nonlinear optical molecules [23]. The polar axis of HMB-TMS crystals is defined as the average direction of the maximal first-order hyperpolarizability β_{\max} of HMB (2-(4-hydroxy-3-methoxystyryl)-3-methylbenzo[d]thiazol-3-ium) molecular cations [28]. HMB-TMS crystals have a large diagonal component of the macroscopic second-order nonlinear optical response

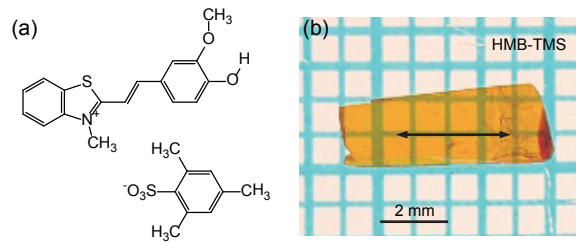


Fig. 1. (a) Chemical structure of HMB-TMS. (b) Photograph of a cleaved HMB-TMS crystal. The arrow indicates the crystal polar axis and the cleavage plane is parallel to the paper.

($\beta_{111}^{\text{eff}} \geq 162 \times 10^{-30}$ esu or 679×10^{-40} m⁴/V) [28], which is very promising for highly efficient THz generation with pump light polarized along the crystal polar axis.

We measured the absorption and refractive/group indices of HMB-TMS crystals along the crystal polar axis along which we expect optimal THz generation efficiency. As measured in the optical transmittance spectrum from our previous work [28], HMB-TMS crystals have very good transparency across the spectral range between 580 and 1620 nm. The optical group indices along the polar axis of HMB-TMS crystals at several wavelengths in the NIR regime between 1200 and 1450 nm were measured here using an autocorrelation method based on noncollinear second harmonic generation (details can be found in [29]). The refractive indices and power absorption coefficients along the polar axis of HMB-TMS crystals between 0.5 and 5.5 THz were measured using a THz time-domain spectroscopy system. The results are shown in Figs. 2(a) and 2(b) where the values are averaged data measured from two crystals having different thickness and the uncertainties are the differences which mainly originate from uncertainties in crystal thickness measurements and different crystal qualities. As shown in the THz power absorption coefficients in Fig. 2(a), HMB-TMS has an overall moderate absorption across the measured spectral range which shows relatively better THz transparency compared to other organic crystals such as OH1 [30]. There are several phonon absorptions at approximately 1.8, 3.6, 4.1 and 5.4 THz.

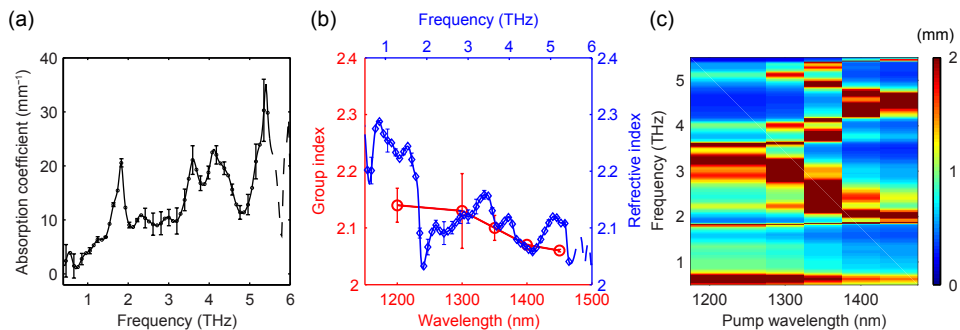


Fig. 2. (a) Power absorption coefficients of HMB-TMS crystals (black solid line). (b) Optical group indices at selected wavelengths between 1200 and 1450 nm (red line) and THz refractive indices between 0.5 and 5.5 THz (blue solid line) of HMB-TMS crystals. All the results are averaged data from measurements of two different crystals and the error bar indicates the differences. The THz data represented by dashed lines are below the noise floor. (c) Optimum crystal lengths calculated at the measured pump wavelengths and THz frequencies. Values above 2 mm are saturated in the color coding.

The measured optical and THz indices are plotted in Fig. 2(b). Though the HMB-TMS crystals show considerable dispersion due to the phonons, the overall good matching between the THz

and optical indices indicates good phase matching between NIR and THz fields in the crystals. Quantitatively, THz generation efficiency by OR is approximately described by the effective generation length as follows [31, 32],

$$l_{\text{gen}}(\nu, \lambda, l) = \sqrt{\frac{e^{-\alpha_{\text{THz}}(\nu)l} + e^{-2\alpha_{\text{opt}}(\lambda)l} - 2e^{-\alpha_{\text{opt}}(\lambda)l - \alpha_{\text{THz}}(\nu)l/2} \cos[\pi l / l_{\text{coh}}(\nu, \lambda)]}{[\alpha_{\text{THz}}(\nu)/2 - \alpha_{\text{opt}}(\lambda)]^2 + [\pi / l_{\text{coh}}(\nu, \lambda)]^2}} \quad (1)$$

where $\alpha_{\text{THz}}(\nu)$ and $\alpha_{\text{opt}}(\lambda)$ are the absorption coefficients at THz fields at frequency ν and optical fields at wavelength λ , $l_{\text{coh}}(\nu, \lambda) = c / (2\nu |n_{\text{THz}}(\nu) - n_g(\lambda)|)$ is the coherence length for THz and optical fields, c is the speed of light in vacuum, and $n_{\text{THz}}(\nu)$ and $n_g(\lambda)$ are the refractive and group indices for THz and optical fields, respectively. The optimum crystal length is defined as the shortest crystal length that maximizes the effective generation length shown in Eq. (1). Due to the absence of the optical absorption coefficients data, we assume that $\alpha_{\text{opt}}(\lambda) = 0$ in Eq. (1), which is justifiable by the high transparency measured in ref. [28].

The calculated optimum crystal lengths are plotted in Fig. 2(c). The large optimum crystal lengths indicate excellent phase matching between broadband THz fields and optical pump fields between 1200 and 1450 nm, which allows efficient OR in collinear geometry. As the pump wavelength increases, phase matching is more favorable for higher frequency components. Due to finite THz absorption by phonons, the crystal thickness optimal for the most efficient THz generation is smaller than that expected by coherence lengths. The optimal crystal thickness and pump wavelength are determined experimentally in the next sections.

3. Experimental setup

The experimental setup is shown schematically in Fig. 3. NIR pulses centered between 1200 and 1450 nm were delivered by an optical parametric amplifier (TOPAS, Light Conversion) that was pumped by a Ti:Sapphire amplifier (Legend, Coherent). The beams were sent through a 2-mm aperture to yield similar sizes incident on different HMB-TMS crystals which also had a 2-mm aperture. The optical polarization was parallel to the crystal polar axis. The generated THz pulses propagated collinearly with the NIR pulses. Using a pair of 90-degree off-axis parabolic mirrors (PMs), the THz pulses were collimated and focused onto a GaP crystal for electro-optic sampling (EOS) [33] measurements of the THz waveform and electric field strength, while the residual NIR light was completely blocked by a black Teflon sheet. To avoid thermal damage in the HMB-TMS crystals, the NIR beam was modulated at 71.43 Hz to decrease the average power on the crystals.

A weak 90-fs laser pulse at 800 nm was time-delayed and spatially overlapped with the THz focus. A 0.1-mm thick free-standing (110)-cut GaP crystal was placed at the THz focus for EOS, which could provide a detection bandwidth up to 6 THz [34]. The depolarization of the gate pulses induced by THz electric fields in the GaP crystal was measured by a quarter wave-plate, a Wollaston prism and a pair of balanced photodiodes. The measured transient THz electric field strength is given by,

$$E_{\text{THz}} = \frac{\lambda}{2\pi n^3 r_{41} t_{\text{GaP}} L} \sin^{-1}\left(\frac{\Delta I}{I}\right) \quad (2)$$

where $\lambda = 800$ nm is the wavelength of the gate pulse, $n = 3.2$ is the refractive index of GaP at 800 nm, $r_{41} = 0.88$ pm/V is the electro-optic coefficient of GaP, $t_{\text{GaP}} = 0.46$ is the Fresnel transmission coefficient for THz fields from air to GaP, L is the GaP crystal thickness, ΔI is the intensity difference between the vertical and horizontal polarization components of the gate pulse, and I is the sum of them [15].

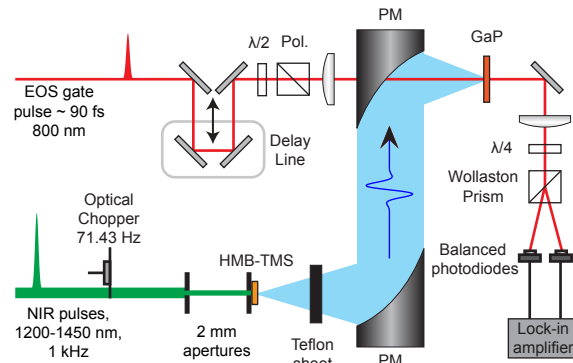


Fig. 3. Experimental setup used for THz generation in HMB-TMS crystals. NIR pulses between 1200 and 1450 nm at 1-kHz repetition rate were incident onto the HMB-TMS crystal in collinear geometry. The generated THz pulses were collimated and focused onto a GaP crystal by a pair of 3-inch diameter parabolic mirrors (PMs) with effective focal lengths of 7 and 3 inches. 800 nm gate pulses were time delayed, attenuated by a half wave-plate ($\lambda/2$) and polarizer, and overlapped with the THz pulses at the GaP crystal for electro-optic sampling (EOS).

4. Efficient THz generation in HMB-TMS crystals

THz generation experiments were conducted on HMB-TMS crystals with different thicknesses between 0.26 and 1.05 mm at each available NIR pump wavelength to test the THz generation efficiency. For a fair comparison, the pump pulses at each selected wavelength incident on the crystals had the similar sizes, and the pulse energies were set to 80 μJ in all measurements. The peak THz electric fields were characterized according to Eq. (2). The peak THz electric field for each crystal thickness at each pump wavelength were measured separately and are summarized in Fig. 4(a). Among the seven crystals measured, the crystal with a thickness of 0.4 mm shows the maximum peak THz electric field strength of 200 kV/cm at a pump wavelength of 1350 nm. The THz time-domain waveforms generated by the 0.4-mm thick HMB-TMS crystal at each pump wavelength are shown in Fig. 4(b). As wavelength increases, the THz pulse becomes slightly narrower in time. The oscillatory features following the main pulse originate from the phonons in the HMB-TMS crystal. Numerical Fourier transformation of the THz waveforms gives rise to the THz spectra, and the Fourier-transform (FT) amplitude spectra are shown in Fig. 4(c). The THz spectra become broader and the maximum spectral amplitude shifts to higher frequencies between 2 and 3 THz as the pump wavelength increases, which is consistent with the trend shown by the coherence lengths at these wavelengths.

The THz generation efficiency of the 0.4-mm HMB-TMS crystal was further studied by measuring the peak THz electric field as a function of pump pulse energy at 1350 nm, which is plotted in Fig. 5(a). At low pump energy, the peak field shows a nearly linear dependence on the pump pulse energy, which is as expected from the second-order OR process. As pump energy increases, a sublinear dependence appears which indicates saturation of OR. It may be attributed to multiphoton (3-photon) absorption [35], as the bandgap of HMB-TMS is about 2.5 eV (500 nm in wavelength) [28]. At the highest available pump pulse energy of 430 μJ , the peak THz electric field reaches as high as 0.66 MV/cm.

Another important parameter characterizing the THz generation efficiency is the optical-to-THz energy conversion efficiency. To measure the conversion efficiency, we used a pyroelectric detector (Microtech) to measure the THz energy at the focus of the second PM as a function of the incident pump pulse energy. The conversion efficiency was obtained by dividing the THz energy by the incident pump energy. The results are plotted in Fig. 5(b). The THz energy shows

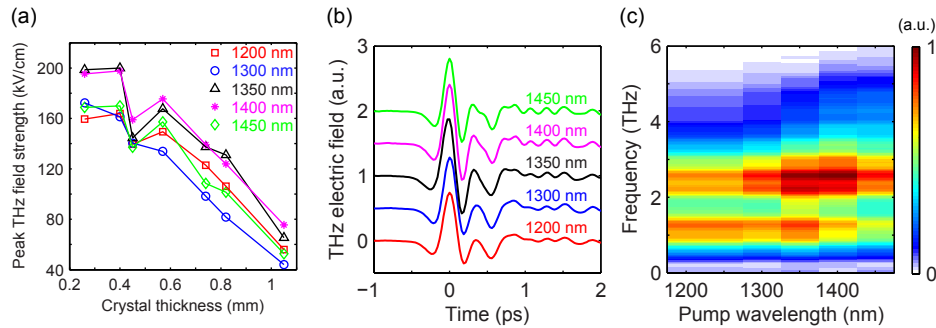


Fig. 4. (a) Peak THz electric field strength measured for HMB-TMS crystals with various thicknesses at each pump wavelength. (b) Single-cycle THz time-domain waveforms generated from the 0.4-mm thick crystal at each pump wavelength measured by EOS. (c) FT amplitude spectra of the THz fields in (b) at each pump wavelength. As the pump wavelength increases, the spectra become broader and the maximum amplitude shifts to higher frequencies.

a quadratic dependence at low incident pump pulse energy, consistent with Fig. 5(a). As a result, the conversion efficiency within this range shows a linear increase. At higher pump energies, the onset of saturation results in a quasi-linear increase in the THz energy potentially due to 3-photon absorption. The conversion efficiency reaches a plateau regime when the pump energy exceeds 200 μJ . At the highest pump energy of 430 μJ , the THz energy was measured to be 1 μJ , and the corresponding conversion efficiency reaches 0.23%. The pyroelectric detector has a decrease in the responsivity as the measured frequency increases, which is not considered here. The values reported here hence may represent a lower bound on the THz energy and conversion efficiency from the HMB-TMS crystal.

The time-domain waveform and FT amplitude spectrum at the highest pump pulse energy of 430 μJ are plotted in Figs. 5(c) and 5(d). As shown in Fig. 5(c), single-cycle THz pulses with a peak electric field of 0.66 MV/cm are located at ~ 0 ps, which is followed by oscillatory features due to the phonons in the crystal. The FT amplitude spectrum shown in the lower panel of Fig. 5(d) indicates a broad bandwidth that spans from 0.1 to 5.4 THz. We also measured the THz transmission of the Teflon sheet that was used to block the residual pump light in the experiment. The transmission coefficient is shown in the upper panel of Fig. 5(d), which indicates a cut-off frequency at ~ 5.5 THz. The bandwidth of the THz pulses generated from the HMB-TMS crystal is largely limited by this Teflon sheet. The THz field strength and bandwidth are hence estimated to be even higher after correction for the Teflon sheet.

Using large-area crystals could drastically increase the THz energy and field strength under the current pump fluence. For example, increasing the crystal size by a factor of two, which is technologically feasible by using a single crystal or a partitioned crystal [26], could result in an increase in the THz energy (field) by a factor of four (two), which could readily achieve MV/cm-level THz field strengths. The THz bandwidths in the current measurements were all limited to be below 6 THz due to a Teflon sheet in the THz beam path used to block the residual pump light. The real THz bandwidth is expected to be much larger. Using pump pulses at longer wavelengths could increase the THz bandwidth due to better phase matching for higher THz frequencies. The saturation level of the pump power can also be increased due to reduced multiphoton absorption at longer wavelengths [35,36]. For example, when the pump wavelength is longer than 1500 nm, 4-photon absorption instead of the current 3-photon absorption becomes the lowest order. THz generation in HMB-TMS crystals with these considerations is worth further exploration.

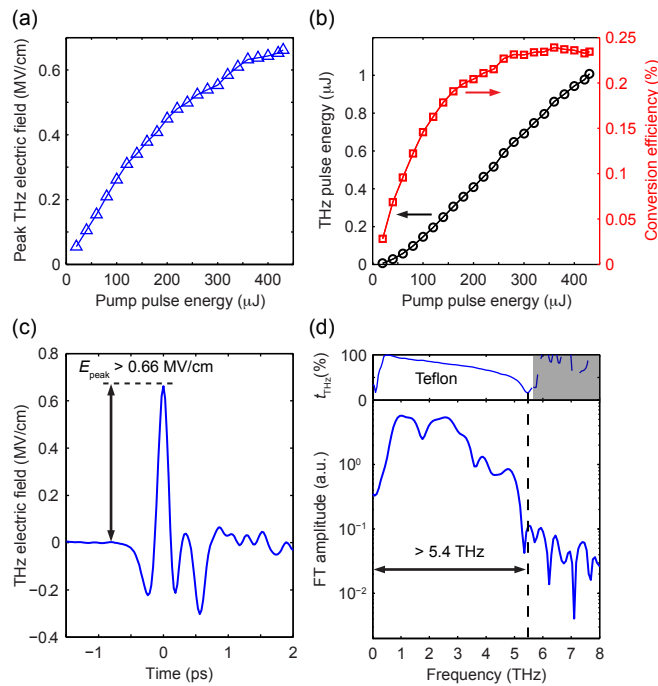


Fig. 5. (a) Peak THz electric field generated by the 0.4-mm HMB-TMS crystal as a function of incident pump pulse energy at 1350 nm. (b) THz pulse energy (black circles) and pump-to-THz energy conversion efficiency (red squares) measured as functions of incident pump pulse energy. (c) THz time-domain waveform with a peak electric field of 0.66 MV/cm generated from the 0.4-mm HMB-TMS crystal. (d) Upper panel shows the THz transmission coefficients of the Teflon sheet used in the experiment. It shows a cut-off frequency at ~5.5 THz. The data in the shaded area is below the noise floor. Lower panel shows the THz FT amplitude spectrum spanning from 0.1 to 5.4 THz. The bandwidth is largely limited by the Teflon.

5. Conclusions

In summary, we have studied the THz generation properties of the highly nonlinear organic HMB-TMS crystals. The optical and THz properties of HMB-TMS were measured and proved favorable for efficient THz generation by OR with collinear phase matching. Strong THz fields were demonstrated from HMB-TMS crystals pumped by NIR pulses from an OPA. A 0.4-mm thick HMB-TMS crystal with a small clear aperture of 2 mm was capable of generating strong THz fields reaching 0.66 MV/cm when the crystal was pumped by NIR fs pulses at 1350 nm. The THz energy was measured to be 1 μJ at a pump energy of 430 μJ, which corresponded to a pump-to-THz energy conversion efficiency of 0.23%. The intense and broadband THz pulses generated by the HMB-TMS crystals in a simple collinear experimental geometry permit wide-ranging applications in THz spectroscopy and optics.

Funding

Office of Naval Research (ONR) (N00014-13-1-0509) and Defense University Research Instrumentation Program (DURIP) (N00014-15-1-2879); the Samsung Global Research Outreach (GRO) program; National Research Foundation of Korea (NRF) funded by the Ministry of Science, ICT & Future Planning and Ministry of Education, Korea (No. 2016R1A2B4011050, 2014R1A5A1009799, 2015K1A3A1A14004646, and 2009-0093826).

References

1. T. Kampfrath, K. Tanaka, and K. A. Nelson, "Resonant and nonresonant control over matter and light by intense terahertz transients," *Nat. Photonics* **7**, 680–690 (2013).
2. H. Y. Hwang, S. Fleischer, N. C. Brandt, B. G. Perkins Jr, M. Liu, K. Fan, A. Sternbach, X. Zhang, R. D. Averitt, and K. A. Nelson, "A review of non-linear terahertz spectroscopy with ultrashort tabletop-laser pulses," *J. Mod. Opt.* **62**, 1447–1479 (2015).
3. M. Liu, H. Y. Hwang, H. Tao, A. C. Strikwerda, K. Fan, G. R. Keiser, A. J. Sternbach, K. G. West, S. Kittiwatanakul, J. Lu, S. A. Wolf, F. G. Omenetto, X. Zhang, K. A. Nelson, and R. D. Averitt, "Terahertz-field-induced insulator-to-metal transition in vanadium dioxide metamaterial," *Nature* **487**, 345–348 (2012).
4. S. Fleischer, Y. Zhou, R. W. Field, and K. A. Nelson, "Molecular orientation and alignment by intense single-cycle THz pulses," *Phys. Rev. Lett.* **107**, 163603 (2011).
5. S. Fleischer, R. W. Field, and K. A. Nelson, "Commensurate two-quantum coherences induced by time-delayed THz fields," *Phys. Rev. Lett.* **109**, 123603 (2012).
6. I. Katayama, H. Aoki, J. Takeda, H. Shimamoto, M. Ashida, R. Kinjo, I. Kawayama, M. Tonouchi, M. Nagai, and K. Tanaka, "Ferroelectric soft mode in a SrTiO₃ thin film impulsively driven to the anharmonic regime using intense picosecond terahertz pulses," *Phys. Rev. Lett.* **108**, 097401 (2012).
7. M. A. Allodi, I. A. Finneran, and G. A. Blake, "Nonlinear terahertz coherent excitation of vibrational modes of liquids," *J. Chem. Phys.* **143**, 234204 (2015).
8. C. Vicario, C. Ruchert, F. Ardana-Lamas, P. M. Derlet, B. Tudu, J. Luning, and C. P. Hauri, "Off-resonant magnetization dynamics phase-locked to an intense phase-stable terahertz transient," *Nat. Photonics* **7**, 720–723 (2013).
9. T. Kubacka, J. A. Johnson, M. C. Hoffmann, C. Vicario, S. De Jong, P. Beaud, S. Grübel, S.-W. Huang, L. Huber, L. Patthey, Y.-D. Chuang, J. J. Turner, G. L. Dakovski, W.-S. Lee, M. P. Minitti, W. Schlotter, R. G. Moore, C. P. Hauri, S. M. Koochpayeh, V. Scagnoli, G. Ingold, S. L. Johnson, and U. Staub, "Large-amplitude spin dynamics driven by a THz pulse in resonance with an electromagnon," *Science* **343**, 1333–1336 (2014).
10. S. Baierl, J. H. Mentink, M. Hohenleutner, L. Braun, T.-M. Do, C. Lange, A. Sell, M. Fiebig, G. Woltersdorf, T. Kampfrath, and R. Huber, "Terahertz-driven nonlinear spin response of antiferromagnetic nickel oxide," *Phys. Rev. Lett.* **117**, 197201 (2016).
11. J. Lu, Y. Zhang, H. Y. Hwang, B. K. Ofori-Okai, S. Fleischer, and K. A. Nelson, "Nonlinear two-dimensional terahertz photon echo and rotational spectroscopy in the gas phase," *Proc. Natl. Acad. Sci.* **113**, 11800–11805 (2016).
12. I. A. Finneran, R. Welsch, M. A. Allodi, T. F. Miller, and G. A. Blake, "Coherent two-dimensional terahertz-terahertz-raman spectroscopy," *Proc. Natl. Acad. Sci.* **113**, 6857–6861 (2016).
13. J. Lu, X. Li, H. Y. Hwang, B. K. Ofori-Okai, T. Kurihara, T. Suemoto, and K. A. Nelson, "Coherent two-dimensional terahertz magnetic resonance spectroscopy of collective spin waves," *Phys. Rev. Lett.* **118**, 207204 (2017).
14. K.-L. Yeh, M. Hoffmann, J. Hebling, and K. A. Nelson, "Generation of 10 μ J ultrashort terahertz pulses by optical rectification," *Appl. Phys. Lett.* **90**, 171121 (2007).
15. H. Hirori, A. Doi, F. Blanchard, and K. Tanaka, "Single-cycle terahertz pulses with amplitudes exceeding 1 MV/cm generated by optical rectification in LiNbO₃," *Appl. Phys. Lett.* **98**, 091106 (2011).
16. J. A. Fülöp, Z. Ollmann, C. Lombosi, C. Skrobol, S. Klingebiel, L. Pálfalvi, F. Krausz, S. Karsch, and J. Hebling, "Efficient generation of THz pulses with 0.4 mJ energy," *Opt. Express* **22**, 20155–20163 (2014).
17. X.-J. Wu, J.-L. Ma, B.-L. Zhang, S.-S. Chai, Z.-J. Fang, C.-Y. Xia, D.-Y. Kong, J.-G. Wang, H. Liu, C.-Q. Zhu, X. Wang, C.-J. Ruan, and Y.-T. Li, "Highly efficient generation of 0.2 mJ terahertz pulses in lithium niobate at room temperature with sub-50 fs chirped Ti: sapphire laser pulses," *Opt. Express* **26**, 7107–7116 (2018).
18. J. Hebling, G. Almási, I. Z. Kozma, and J. Kuhl, "Velocity matching by pulse front tilting for large-area THz-pulse generation," *Opt. Express* **10**, 1161–1166 (2002).
19. J. A. Fülöp, L. Pálfalvi, G. Almási, and J. Hebling, "Design of high-energy terahertz sources based on optical rectification," *Opt. Express* **18**, 12311–12327 (2010).
20. S.-W. Huang, E. Granados, W. R. Huang, K.-H. Hong, L. E. Zapata, and F. X. Kärtner, "High conversion efficiency, high energy terahertz pulses by optical rectification in cryogenically cooled lithium niobate," *Opt. Lett.* **38**, 796–798 (2013).
21. K.-Y. Kim, A. J. Taylor, J. H. Glowina, and G. Rodriguez, "Coherent control of terahertz supercontinuum generation in ultrafast laser–gas interactions," *Nat. Photonics* **2**, 605–609 (2008).
22. C. Vicario, C. Ruchert, and C. P. Hauri, "High field broadband THz generation in organic materials," *J. Mod. Opt.* **62**, 1480–1485 (2015).
23. L. R. Dalton, P. Günter, M. Jazbinšek, P. A. Sullivan, and O.-P. Kwon, *Organic Electro-Optics and Photonics: Molecules, Polymers and Crystals* (Cambridge University, 2015).
24. M. Shalaby and C. P. Hauri, "Demonstration of a low-frequency three-dimensional terahertz bullet with extreme brightness," *Nat. Commun.* **6**, 5976 (2015).
25. C. Vicario, B. Monoszlai, M. Jazbinšek, S.-H. Lee, O.-P. Kwon, and C. P. Hauri, "Intense, carrier frequency and bandwidth tunable quasi single-cycle pulses from an organic emitter covering the Terahertz frequency gap," *Sci. Rep.* **5**, 14394 (2015).
26. C. Vicario, B. Monoszlai, and C. P. Hauri, "GV/m single-cycle terahertz fields from a laser-driven large-size partitioned organic crystal," *Phys. Rev. Lett.* **112**, 213901 (2014).

27. S.-H. Lee, M. Jazbinšek, C. P. Hauri, and O.-P. Kwon, "Recent progress in acentric core structures for highly efficient nonlinear optical crystals and their supramolecular interactions and terahertz applications," *Cryst. Eng. Comm.* **18**, 7180–7203 (2016).
28. S.-H. Lee, J. Lu, S.-J. Lee, J.-H. Han, C.-U. Jeong, S.-C. Lee, X. Li, M. Jazbinšek, W. Yoon, H. Yun, B. J. Kang, F. Rotermund, K. A. Nelson, and O.-P. Kwon, "Benzothiazolium single crystals: A new class of nonlinear optical crystals with efficient thz wave generation," *Adv. Mater.* **29**, 1701748 (2017).
29. A. Schneider, F. D. J. Brunner, and P. Günter, "Determination of the refractive index over a wide wavelength range through time-delay measurements of femtosecond pulses," *Opt. Commun.* **275**, 354–358 (2007).
30. F. D. Brunner, O.-P. Kwon, S.-J. Kwon, M. Jazbinšek, A. Schneider, and P. Günter, "A hydrogen-bonded organic nonlinear optical crystal for high-efficiency terahertz generation and detection," *Opt. Express* **16**, 16496–16508 (2008).
31. A. Schneider, M. Neis, M. Stillhart, B. Ruiz, R. U. Khan, and P. Günter, "Generation of terahertz pulses through optical rectification in organic DAST crystals: theory and experiment," *J. Opt. Soc. Am. B* **23**, 1822–1835 (2006).
32. J. Lu, H. Y. Hwang, X. Li, S.-H. Lee, O.-P. Kwon, and K. A. Nelson, "Tunable multi-cycle THz generation in organic crystal HMQ-TMS," *Opt. Express* **23**, 22723–22729 (2015).
33. Q. Wu and X.-C. Zhang, "Free-space electro-optic sampling of terahertz beams," *Appl. Phys. Lett.* **67**, 3523–3525 (1995).
34. S. Casalbuoni, H. Schlarb, B. Schmidt, P. Schmüser, B. Steffen, and A. Winter, "Numerical studies on the electro-optic detection of femtosecond electron bunches," *Phys. Rev. Spec. Top. Accel. Beams* **11**, 072802 (2008).
35. M. C. Hoffmann, K.-L. Yeh, J. Hebling, and K. A. Nelson, "Efficient terahertz generation by optical rectification at 1035 nm," *Opt. Express* **15**, 11706–11713 (2007).
36. G. Polónyi, B. Monoszlai, G. Gäumann, E. J. Rohwer, G. Andriukaitis, T. Balciunas, A. Pugzlys, A. Baltuska, T. Feurer, J. Hebling, and J. A. Fülöp, "High-energy terahertz pulses from semiconductors pumped beyond the three-photon absorption edge," *Opt. Express* **24**, 23872–23882 (2016).